Tribo-Mechanical Evaluations of Cobalt-Based (Stellite 4) Alloys Manufactured via HIPing and Casting

H. Yu, R. Ahmed*, H. de Villiers Lovelock, and S. Davies

Abstract— **Cobalt-based alloys are known for their excellent wear resistance, particularly under high temperature and corrosive environments. However the cast cobalt-based alloys have relatively high brittleness, and low toughness, due to their coarse carbide structure. This paper aims to comprehend if carbide refinement, caused by changing the processing route from sand casting to powder consolidated Hot Isostatic Pressing (HIPing), can improve the tribo-mechanical properties of cobalt-based alloys. The alloy selected for this investigation had a nominal wt.% composition of Co-30Cr-14W-1C, which is similar to the composition of the commercially available Stellite®4 alloy. The Hot Isostatic Pressed (HIPed) alloy had a much finer microstructure than the cast alloy, which showed a typical hypoeutectic dendritic microstructure. Both alloys had similar hardness. Although the cast alloy showed slightly better abrasive and sliding wear resistance than the HIPed alloy due to their coarser eutectic carbides, the HIPed alloy had a significant advantage on the impact toughness and contact fatigue performance. The results of this comparative investigation indicated that the HIPed alloy had an attractive combination of tribo-mechanical properties, i.e. improved impact and fatigue resistance, whilst preserving the high hardness and good wear resistance associated with the cast alloy, making it suitable for relatively higher stress applications.**

Index Terms— **Fatigue; HIPing; Stellite 4; Wear**

I. INTRODUCTION

The cobalt-based alloys, which are generally known as Stellite [1] alloys, are widely used in industry due to their excellent wear resistance, and the ability to retain high strength at elevated temperatures. The properties of cobalt-based alloys are derived from the sluggish phase transformation (F.C.C. to H.C.P.) of Co, solid solution strengthening by W/Mo, and the formation of hard carbides [1]-[5]. The alloy selected for this investigation had a nominal wt.% composition of Co-30Cr-14W-1C, which was similar to the commercially available Stellite®4 alloy. Applications of this alloy include dies for hot pressing and extrusion. The relatively high tungsten content and low carbon content of this alloy ensures that sufficient tungsten is retained in the solid solution, instead of being depleted to form carbides. Therefore this alloy can maintain good hardness and strength at elevated temperatures.

Cobalt-based alloys can be used as castings, powder metallurgy (P/M) parts, Hot Isostatic Pressed (HIPed) consolidated parts, weld hard-facings, laser hard-facings and thermal spray coatings [1], [2], [6]. Although the cast alloys have had extensive usage since their introduction in 1910's, the relatively coarser carbide structure and the presence of defects such as porosity within the castings often result in high brittleness and low impact and fatigue resistance. Carbide refinement by varying the processing route from casting to Hot Isostatic Pressing (HIPing) is one way to improve the combined properties of cobalt-based alloys. The HIPing process involves the simultaneous application of high temperature (up to 2000ºC), and pressure (up to 200 MPa) in a HIPing vessel.

Although the structure-property relationships of cobalt-based alloys have been a topic of research for a number of investigations [4]-[9], comparative studies between the alloys produced via different processing routes (especially HIPing) are limited. Hence this paper aims to conduct a comparative investigation of the structure-property relationships between the alloys produced via sand casting and powder consolidated HIPing. Results of this investigation are discussed on the basis of the microstructural examination via Scanning Electron Microscopy (SEM), and tribo-mechanical evaluations including hardness, impact toughness, abrasive wear, sliding wear, and contact fatigue resistance.

II. EXPERIMENTAL TEST PROCEDURE

A. Materials and Microstructure

The cast alloys under the current investigation were sand castings. The HIPed alloys were produced from the gas-atomised powders and consolidated in the HIPing vessel at a temperature and pressure of 1200˚C and 100 MPa, respectively, for four hours. The sieve analysis (+250 μm: 0.0wt.%, +180 μm: 0.2wt.%, +125 μm: 2.3wt.%, +45 μm:

72.5wt.%, -45 μm: 25.1wt.%) indicated that more than 97wt.% of the powder particles had a size smaller than 125 μm. Table I summarises the chemical compositions of both alloys. The microstructure of the powders and both alloys was observed via SEM using a back-scattered electron imaging detector. The chemical compositions of different phases developed in the powders and alloys were determined via Energy Dispersive X-ray Spectroscopy (EDS) and X-Ray Diffractometry (XRD) with Cu-K_α radiation (x-ray wavelength = 1.5406 Å). Image analysis was also conducted to ascertain the area fractions of individual phases.

B. Hardness and Unnotched Charpy Impact Tests

A conventional Avery Vickers hardness tester was used to measure the macrohardness under a load of 294 N. The Vickers microhardness was measured using a MVK-H1 tester under a load of 2.94 N. Five macrohardness measurements and ten microhardness measurements were conducted on each alloy. In order to investigate the microhardness of individual phases in the cast alloy, ten tests under a low load of 0.098 N were also conducted. Three unnotched Charpy impact tests were conducted on each alloy. The test samples had dimensions of 10 mm × 10 mm × 55mm. The test procedure was similar to that specified by the ASTM E23-94b standard [10], except that the samples were unnotched due to their high brittleness.

C. Abrasive Wear Tests

The Dry Sand Rubber Wheel (DSRW) abrasion tests were conducted following the procedure specified by the ASTM G65 standard (Procedure B) [11]. Three tests were conducted on each alloy. During the tests, the alloy sample (6 mm × 25 mm × 75 mm) was forced under a load of 130 N against the rubber wheel (228.6 mm in diameter), which rotated at a speed of 200 ± 5 rpm. Two types of silica sand were used as abrasives in this investigation. Both were dry and rounded, but they were different in size distribution. At least 85wt.% of particles for sand A had a size distribution in the range of 90-180 μm. Sand B had a larger average particle size, with at least 85wt.% particles having a size distribution between 150 μm and 300 μm. The sand particles were introduced between the alloy sample and the rubber wheel at a flow rate of 330 g/min. Each test lasted for a total of 2000 revolutions.

D. Sliding Wear Tests

The reciprocating ball-on-flat sliding wear tests were conducted following the procedure specified in the ASTM G133 standard [12]. These tests were conducted between a tungsten carbide ball (93.5-94.5wt.% WC, and 5.5-6.5wt.% Co) and the alloy disc sample under a normal load of 25 N. The WC-Co ball had a radius of 6.35 mm and a hardness of HRA 91. The alloy disc sample had a diameter of 31 mm and a thickness of 8 mm. During the tests, the alloy disc experienced reciprocating sliding motion at an oscillating frequency of 1.0 Hz, with a stroke length of 10 mm. Three tests were conducted on each alloy, and the total sliding distance in each test was 500 m. The wear volume loss of the disc sample was computed

from the stroke length and the average cross-sectional area of the wear groove, which was measured via an interferometer.

E. Rolling Contact Fatigue Tests

The Rolling Contact Fatigue (RCF) tests were conducted using a modified four-ball machine. Fig. 1 shows a schematic of the test configuration, in which the alloy disc sample, with a diameter of 31 mm, was held in the drive shaft and drove three planetary Si_3N_4 ceramic balls, with a diameter of 4.75 mm. The three balls were equispaced at 120° using a polymer spacer. The rotary speed of the drive shaft was set at 5000 ± 5 rpm during the tests, and the total contact load was varied as 45 N, 115 N, and 240 N, which resulted in a contact stress of 2.3 GPa, 3.1 GPa, and 4.0 GPa, respectively. Exxon Turbo 2389 was used as the lubricant. The ratio of the Elasto-Hydrodynamic Lubrication (EHL) film thickness to the average surface roughness of the contacting bodies was approximated between 1.4 and 1.8, indicating that the tests were conducted under the mixed lubrication regime. The failure was detected by the increase in the vibration amplitude of the cup assembly above a preset level. Further details of the test assembly and procedures can be appreciated from Stewart et al. [13].

Table I Chemical compositions of the cast and HIPed alloys (wt.%)

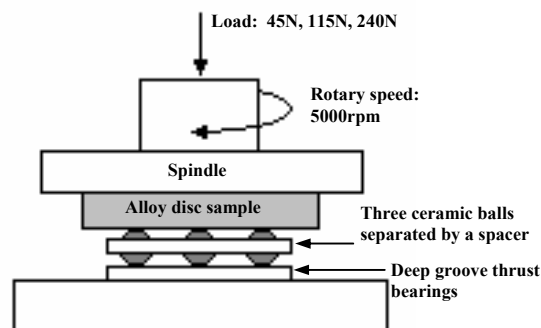|	Co	Cr	W	C	Mo	Fe	Ni	Mn	Si
Cast alloy	Bal.	31.7	13.5	0.90	0.20	1.65	0.65	0.56	0.72
HIPed alloy	Bal.	31.0	14.4	0.67	0.12	2.16	1.82	0.26	1.04

Fig. 1 Schematic illustration of the cup assembly for the rolling contact fatigue tests

III. RESULTS AND DISCUSSION

A. Microstructure and Phase Analysis

The microstructures of the gas atomised powder particles, cast and HIPed alloys are shown in Fig. 2. Fig. 2a shows the dendritic microstructure of the cross-sections of the powder particles used for HIPing. The possible phases in the powders were identified via XRD as α-Co (F.C.C.), Cr, $Cr_{23}C_6$, Co_6W_6C, Co_3W, and Co_7W_6. Fig. 2b shows the hypoeutectic microstructure of the cast alloy, which consists of Co-rich dendrites (dark region), Cr-rich eutectic phase (grey phase), and W-rich carbide (bright phase). Table II presents the image analysis results of the area fractions of various phases in the

cast and HIPed structures. The XRD analysis revealed that α-Co was the primary phase in the Co-rich solid solution, whilst tungsten was also present in the solid solution, which strengthened it by forming the inter-metallic compounds Co_3W and Co_7W_6. The Cr-rich eutectic phase was unlikely to be pure $Cr_{23}C_6$ carbide as identified via the XRD analysis, because the relatively lower carbon content (0.9wt.%) of the alloy could not lead to such high area fraction (27.7%) of carbides. This phase could be a mixture of $Cr_{23}C_6$ carbides and CoCrW solid solution, as the EDS analysis showed that it consisted of small proportions of Co and W, besides Cr and C. The bright phase was identified as W-rich carbide, Co_6W_6C.

The microstructure of the HIPed alloy (Fig. 2c) consisted of three types of phases, which were uniformly distributed in the matrix (dark region, with an area fraction of 65.8%). The EDS analysis revealed that the light grey phase contained around 35% Co, 28% Cr, and 37% W (in wt.%), indicating that this phase was also CoCrW solid solution, which differed from the matrix phase in terms of its tungsten content. The dark grey phase was Cr-rich carbide with an approximate composition of $(Co_{0.22}Cr_{0.70}W_{0.08})_{23}C_6$. The bright phase was identified as W-rich carbide. The XRD analysis indicated that the possible phases in the HIPed alloy were α-Co, Cr_7C_3, $Cr_{23}C_6$, Co_6W_6C, Co_3W, and Co_7W_6. Most of these phases were inherited from the powders, except for the Cr_7C_3, indicating that it was formed during the HIPing process.

In comparison to the cast alloy, the microstructure of the HIPed alloy was not only finer, but also had discrete carbides, instead of the interconnected three-dimensional eutectic net observed in the cast structure. The difference in the microstructure can have a significant influence on the tribo-mechanical properties. As discussed later, the impact toughness and fatigue resistance, which involved failure mechanisms that were dependent upon crack propagation, benefited from the absence of a three-dimensional eutectic net in the HIPed alloy. However, there was a trade-off between these improvements, and the wear resistance of the HIPed alloy, as the difference in carbide morphology caused changes in the wear mechanisms.

B. Hardness

The microhardness and macrohardness results for both alloys are summarised in Table III. It is widely accepted that the contents of carbon and tungsten determine the hardness of cobalt-based alloys by forming carbides (Cr_7C_3, $Cr_{23}C_6$, Co_6W_6C) and inter-metallic compounds (Co_3W, Co_7W_6), which can strengthen the solid solution. Some previous investigations have also indicated that the differences in microstructure could affect the hardness of cobalt-based alloys [4], [14]. However in the current investigation, despite quite different microstructures of both alloys, they had similar macrohardness and microharness. The influence of the processing conditions (e.g. casting or HIPing) and the microstructure of the cobalt-based alloys on hardness was therefore insignificant.
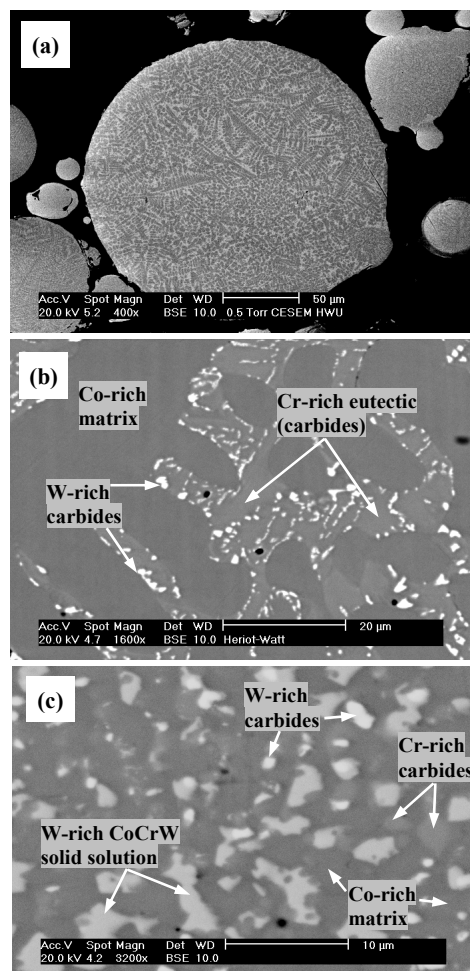

Fig. 2 SEM images showing the microstructure of a) cross-section of the alloy powders; b) cast alloy; c) HIPed alloy

Table II The area fractions of individual phases in the cast and HIPed alloys

	Cast alloy	HIPed alloy
Co-rich matrix	67.5 ± 0.4 %	65.8 ± 1.6 %
W-rich carbides	4.8 ± 0.9 %	2.7 ± 0.2 %
Cr-rich eutectic	27.7 ± 1.4 %	-
Cr-rich carbides	-	15.5 ± 1.4 %
CoCrW solid solution	-	15.1 ± 0.6 %

Table III The hardness and unnotched Charpy impact energy results of cast and HIPed alloys

	Cast alloy	HIPed alloy
Microhardness (HV, 0.098 N)	Cr-rich eutectic: 720.7 ± 82.4 Co-rich matrix: 450.2 ± 51.6	-
Microhardness (HV, 2.94 N)	533.4 ± 13.3	521.5 ± 10.3
Macrohardness (HV, 294 N)	523.4 ± 7.9	538.0 ± 3.2
Unnotched Charpy impact energy (J)	9.83 ± 1.44	21.02 ± 4.23

It was difficult to measure the hardness of individual phases in the HIPed alloy using the Vickers microhardness method, even at a low load of 0.098 N, as the indentation diagonal length was approximately 7 μm, which was larger than the typical carbide particle size (2-5 μm, Fig. 2c) in this alloy. However, the relatively coarser carbide size (10-20 μm) made this assessment feasible in the cast alloy. The average micro-hardness of the eutectic phase in the cast alloy (grey phase in Fig. 2b) was HV 720.7, which was much higher than the hardness of the matrix (HV 450.2), but lower than the typical hardness of pure carbides (HV 1500-2100, [7]). This further confirmed that the eutectic phase was not pure carbide, but a mixture of carbide and CoCrW solid solution. The hardness of the eutectic phase and the matrix in the cast alloy, together with their respective area fractions of 27.7% and 67.5% (Table II), could thus be used to approximate the average hardness of the cast alloy as HV 529, which was very close to the experimental result. This assessment methodology is based upon the assumption that fraction of constituents in multiphase alloys was consistent with the property evaluation, as indicated by Ghar [15].

C. Impact Toughness

The unnotched Charpy impact energy results of the cast and HIPed alloys are shown in Table III. The fractographs of the failed areas after the impact tests are shown in Fig. 3. The cast alloy showed much lower impact energy than the HIPed alloy, which could be attributed to its coarse microstructure. The SEM observations of the fractured cast alloy (Fig. 3a) indicated that brittle fracture took place both within the Cr-rich eutectic phase and at the phase boundaries. Owing to the coarse microstructure, once the cracks initiated, they propagated rapidly along the three-dimensional Cr-rich eutectic net. The HIPed alloy showed a mixture of trans-granular and powder particle boundary fracture, as indicated in Fig. 3b. The cracks followed the boundaries of the carbide phases, and also the powder particle boundaries. The fine HIPed microstructure, along with the matrix ductility, provided a crack arrest mechanism. The crack propagation route had to change direction frequently along the carbide/matrix and in some cases carbide/carbide boundaries, thereby resulting in more energy absorption for the HIPed alloy during the impact tests.

D. Abrasive Wear Performance

Fig. 4 summarises the average abrasive wear volume loss of both alloys. The wear scars after the tests are shown in Fig. 5. Previous investigations have indicated that the abrasive wear resistance of cobalt-based alloys increased with carbide coarsening [16], [17], decreasing abrasive particle size [16], [18], and decreasing abrasive hardness [18]. The cast alloy showed better abrasive wear resistance than the HIPed alloy for both types of sand used in this investigation. The observation of the wear scars revealed that ploughing dominated the wear loss of both alloys.

For the cast alloy, ploughing mainly took place in the Co-rich matrix (Fig. 5a), which had a lower hardness than the Cr-rich

eutectic net. The eutectic net had good wear resistance so that the ploughing was hindered, as indicated by the discontinuous abrasive marks shown in Fig. 5a, where the preserved eutectic net is appreciable even after the wear test. Some pits on the matrix were also formed due to the denting caused by the angularities of sand particles. However, the wear scars of the HIPed alloy (Fig. 5b) indicated excessive ploughing, because the carbides in the HIPed alloy were too fine to withstand ploughing by the abrasive particles. The abrasive particles also caused plastic deformation on the surface, as indicated by the grooves and ridges in Fig. 5b. The width of the grooves was approximately 10 μm, which was larger than the carbide size (2-5 μm), indicating that the carbides were ploughed along with the matrix. Although plastic deformation itself did not result in material removal, however as a result of cyclic plastic deformation caused by the continuous flow of abrasive particles, cracks initiated and propagated beside the ridges, which ultimately resulted in the removal of material.

The cast alloy suffered more wear loss in the tests with sand A in comparison with sand B, whereas the HIPed alloy had the opposite behaviour. This is because the finer abrasive particles (sand A) could enter and plough the matrix region of the cast alloy more easily. As the material removal in the cast alloy was mainly derived from the ploughing on the matrix, the finer abrasive particles resulted in more wear volume loss. Contrary to this, the wear mechanism of the HIPed alloy was simultaneous ploughing of the carbide and matrix. Therefore the coarser abrasive particles, which could cause wider and deeper grooves, resulted in more wear loss in the HIPed alloy.
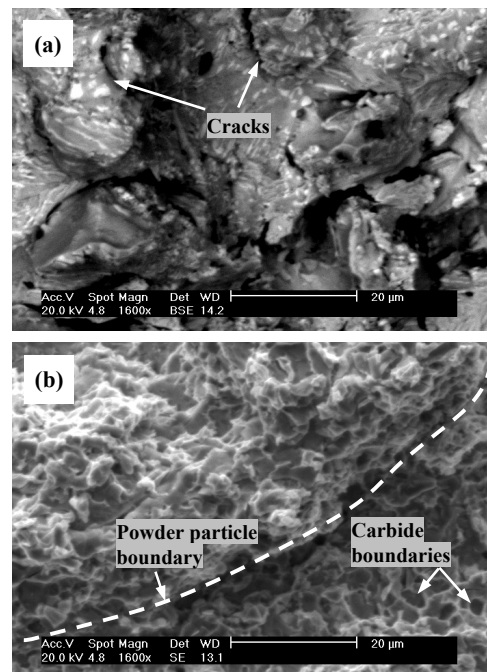

Fig. 3 The fractographs after the unnotched Charpy impact tests on a) cast alloy; b) HIPed alloy
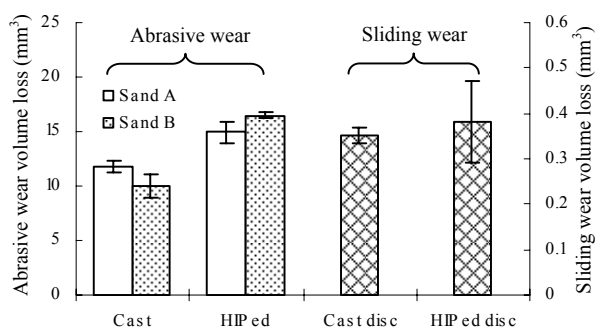
Fig. 4 The wear volume loss of cast and HIPed alloys after the abrasive wear and the sliding wear tests
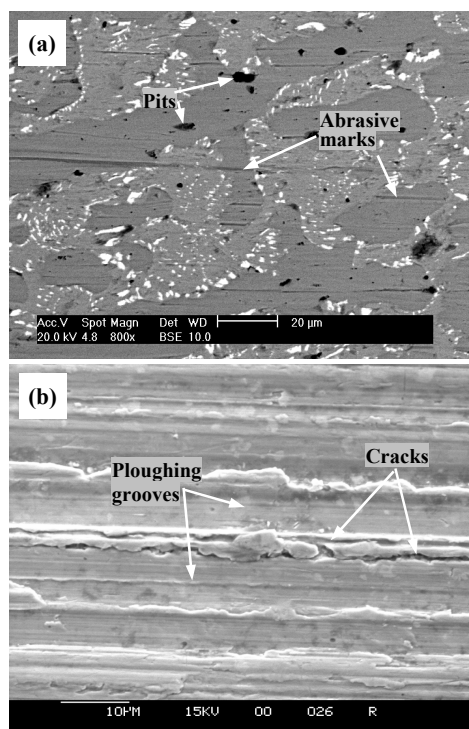

Fig. 5 The wear scars after the abrasive wear tests of a) cast alloy; b) HIPed alloy

E. Sliding Wear Performance

The average volume loss results of the alloy disc samples after the ball-on-flat sliding wear tests are shown in Fig. 4. The wear scars of both alloys are shown in Fig. 6. The WC-Co ball used in this investigation consisted of WC carbides (typically 2 μm in size), which were much smaller than the carbides in the cast alloy, but similar in size to those in the HIPed alloy. Therefore the ball suffered appreciable wear when wearing against the cast alloy, but negligible wear when wearing against the HIPed alloy. Although the cast alloy showed slightly better wear resistance than the HIPed alloy, the total volume loss of the test couples (ball and disc) would be very similar for both alloys due to the relatively higher ball volume loss wearing against the cast alloy. However, the quantitative measurement of the ball material loss could not be accurately performed even

with three-dimensional interferometry, due to the uneven wear on the ball surface.

The grooves and ploughing marks shown in Fig. 6a indicated that ploughing occurred on the matrix of the cast alloy. Some pits were left on the worn surface, probably due to the pullout of the relatively smaller W-rich carbides (bright phase in Fig. 2b). The coarse eutectic net, which was interlocked in the matrix, showed good resistance to ploughing and could be seen intact even after the tests. Ploughing also dominated the volume loss of the HIPed alloy, and caused considerable plastic deformation, as the fine microstructure could not resist ploughing. The grooves shown in Fig. 6b were wide and deep, and ran through the whole length of the wear scar.
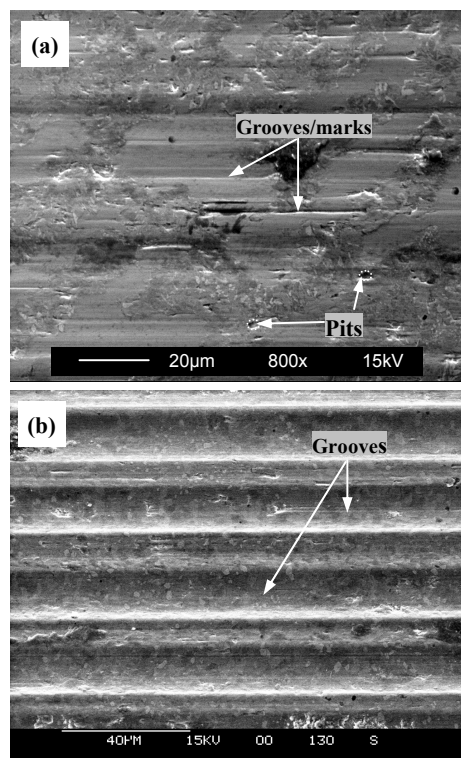

Fig. 6 The wear scars after the sliding wear tests of a) cast alloy; b) HIPed alloy

F. Contact Fatigue Performance

The results of the stress cycles to failure after the RCF tests are summarised in Fig. 7. Tests conducted at 2.3 GPa and 3.1 GPa were suspended after 75.6 million stress cycles without failure. Fig. 8 shows the failed areas of both alloys after the tests conducted at 4 GPa. The HIPed alloy showed better fatigue performance than the cast alloy, particularly under the high stress conditions. The SEM observations of the wear tracks (Fig. 8) indicated that the cast alloy failed via delamination, whereas the HIPed alloy failed via spalling. The failure mechanisms underpinning these failure modes are based upon the theories of surface and subsurface stress risers, further details of which can be appreciated in [19], [20]. Delamination and spalling were caused by the subsurface stress risers, e.g. the orthogonal shear stress and maximum shear stress, which could generally result in crack initiation and propagation in the

subsurface region. Once the subsurface cracks initiated in the cast alloy, they could readily propagate within the coarse eutectic net or at the boundaries. However in the HIPed alloy, the cracks propagated at the carbide boundaries and through the matrix, which hindered the crack propagation and resulted in improved RCF performance.
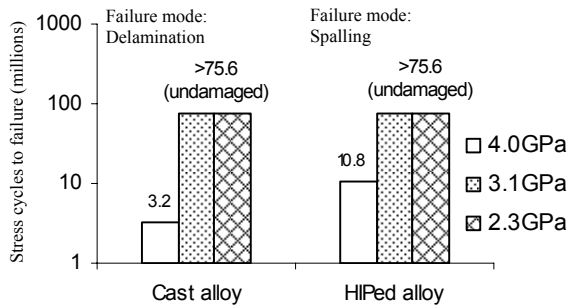

Fig. 7 The stress cycles to failure after rolling contact fatigue tests
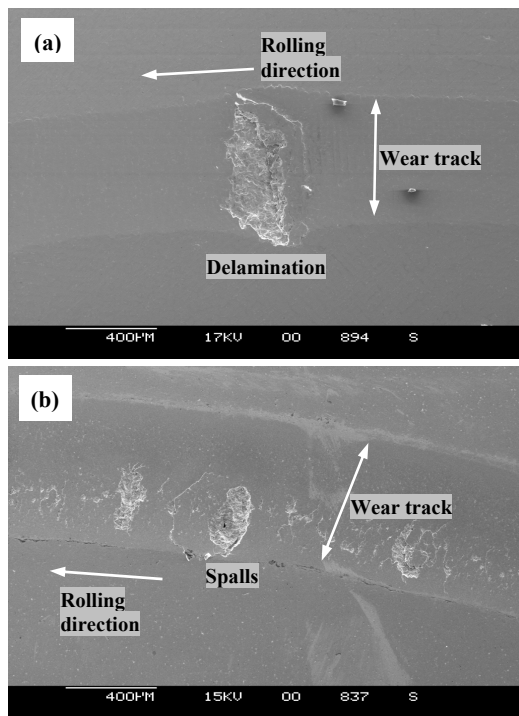

Fig. 8 The wear tracks after the contact fatigue tests (4.0GPa) of a) cast alloy; b) HIPed alloy

IV.   CONCLUSIONS

1)   The HIPed cobalt-based alloy under investigation had a much finer microstructure than the cast alloy. Similar phases, i.e. α-Co, $Cr_{23}C_6$, Co_3W_3C, Co_3W, and Co_7W_6, were identified in both alloys via XRD, whilst Cr_7C_3 was identified in the HIPed alloy only.

2)   Both the cast and HIPed alloys possessed similar hardness, indicating the processing conditions did not affect the hardness significantly.

3)   Benefiting from the absence of the coarse eutectic net, the HIPed alloy showed much higher impact toughness, and improved fatigue resistance than the cast alloy under high stress conditions.

4)   Ploughing was the dominant wear mechanism for both alloys in the abrasive wear and sliding wear tests. The cast alloy showed slightly better wear resistance due to its coarse three-dimensional eutectic, which resisted ploughing.

REFERENCES

[1] P. Crook, "Cobalt and cobalt alloys," *ASM Handbook*, vol. 2, 1991, pp. 446-454.
[2] P. Crook, "Cobalt-base alloys resist wear, corrosion, and heat," *Advanced Materials & Progress*, vol. 145, 1994, pp. 27-30.
[3] K. C. Antony, "Wear-resistant cobalt-based alloys," *Journal of Metals*, vol. 35, 1983, pp. 52-60.
[4] A. Frenk, W. Kurz, "Microstructural effects on the sliding wear resistance of a cobalt-based alloy," *Wear*, vol. 174, 1994, pp. 81-91.
[5] H. Berns, F. Wendl, "Microstructure and properties of CoCr29W (Stellite 6) in the as-cast, forged and powder metallurgical condition," *Proceedings Second International Conference on Cobalt*, 1985, pp. 292-305.
[6] D. L. Klarstrom, "Wrought cobalt-base superalloys," *Journal of Materials Engineering and Performance*, vol. 2, 1993, pp. 523-530.
[7] M. A. Ashworth, J. C. Bryar, M. H. Jacobs, S. Davies, "Microstructure and property relationships in hipped Stellite powders," *Powder Metallurgy*, vol. 42, 1999, pp. 243-249.
[8] J. L. de Brouwer, D. Coutsouradis, "Influence of tungsten and carbon contents on the microstructure and properties of a cobalt-base hardfacing alloy," *Cobalt*, vol. 32, 1966, pp. 141-147.
[9] H. Yu, R. Ahmed, H. de Villiers Lovelock, "A comparison of the tribo-mechanical properties of wear-resistant cobalt-based alloys produced by different manufacturing processes", *ASME Journal of Tribology*, to be published.
[10] ASTM, *Standard Test Methods for Notched Bar Impact Testing of metallic Materials (E23-94b)*, PA: ASTM International, 1994.
[11] ASTM, *Standard Test Method for Measuring Abrasion Using the Dry Sand/Rubber Wheel Apparatus (G65-00)*, PA: ASTM International, 2000.
[12] ASTM, *Standard Test Method for Linearly Reciprocating Ball-on-Flat Sliding Wear (G133-02)*, PA: ASTM International, 2002.
[13] S. Stewart, R. Ahmed, T. Itsukaichi, "Contact fatigue failure evaluation of post-treated WC-NiCrBSi functionally graded thermal sprayed coatings," *Wear*, vol. 257, 2004, pp. 962-983.
[14] V. Kuzucu, M. Ceylan, H. Celik, I. Aksoy, "An investigation of Stellite-6 alloy containing 5.0 wt% silicon," *Journal of Alloys Processing Technology*, vol. 79, 1998, pp. 47-51.
[15] K. Z. Ghar, *Microstructure and Wear of Alloys*, Amsterdam: Elsevier, 1987, pp. 36-37.
[16] P. Crook, A. V. Levy, "Friction and wear of cobalt-base wrought alloys," *ASM Handbook*, vol. 18, 1992, pp. 766-771.
[17] V. M. Desai, C. M. Rao, T. H. Kosel, N. F. Fiore, "Effect of carbide size on the abrasion of cobalt-base powder metallurgy alloys," *Wear*, vol. 94, 1984, pp. 89-101.
[18] T. H. Kosel, S. Z. Li, C. M. Rao, "The size effect in abrasion of dual-phase alloys," *ASLE Transactions*, vol. 28, 1985, pp. 343-350.
[19] R. Ahmed, "Rolling contact fatigue", *ASM Handbook*, vol. 11, W. T. Becker and R. J. Shipley, Eds., 2002, pp. 941-956.
[20] R. Ahmed, M. Hadfield, "Mechanisms of fatigue failure in thermal spray coatings," *Journal of Thermal Spray Technology*, vol. 11, 2002, pp. 333-349.